Spectrochimica Acta Part B 100 (2014) 52–61

Contents lists available at ScienceDirect

Spectrochimica Acta Part B

journal homepage: www.elsevier.com/locate/sab

Discussion of fundamental processes in dielectric barrier discharges used for soft ionization ☆

Vlasta Horvatic [a,*], Cedomil Vadla [a], Joachim Franzke [b]

[a] Institute of Physics, Bijenicka 46, 10000 Zagreb, Croatia
[b] ISAS—Leibniz Institut für analytische Wissenschaften, Bunsen-Kirchhoff-Str. 11, 44139 Dortmund, Germany

ARTICLE INFO

Article history:
Received 26 May 2014
Accepted 25 July 2014

Keywords:
Ambient air ionization
Dielectric barrier discharge
Homogeneous discharge
Filamentary discharge
Rotational temperature

ABSTRACT

Permanent need for simple to apply and efficient methods for molecular mass spectrometry resulted in the development of a variety of methods now commonly termed ambient desorption/ionization mass spectrometry (ADI-MS), which experienced a very rapid development during the last 10 years. The most widely used techniques are direct analysis in real time (DART), plasma assisted desorption/ionization (PADI), flowing afterglow-atmospheric pressure glow discharge ionization (FA-APGDI), low-temperature plasma probe (LTP) and dielectric barrier discharge ionization (DBDI). They all share the advantage of direct, ambient analysis of samples with little or no pretreatment, and employ some kind of electrical discharge to desorb and ionize the analyte species. However, the investigations focused on the characterization, examination and understanding of underlying ionization mechanisms of these discharges are relatively small in number. More efforts are clearly needed in this segment, since the understanding of the fundamentals of these discharges is a prerequisite for optimization of working parameters of ADI-MS sources with the aim of increasing ionization efficiency. Here, ADI-MS techniques will be overviewed, with the emphasis put on the review and the analysis of the recent progress in dielectric barrier discharges utilized for soft ionization.

1. Introduction

Mass spectrometry (MS) constitutes one of the most important and useful analytical instruments. However, unless the investigated species have an intrinsic charge, ionization of the species to be measured is required. Therefore, the realization of efficient ionization has always been crucial for applying mass spectrometry as an analytical tool. Also, the need to monitor samples *in situ* or on real-time basis imposed two additional demands to the technique: possibility to ionize species outside the vacuum chamber of the mass spectrometer and avoidance of any complex sample preparation. These requirements gave rise to the development of numerous ionization techniques (recently reviewed in Refs. [1–12]) now known as ambient desorption/ionization mass spectrometry (ADI-MS), which allows the rapid analysis of samples or objects in their native state in the open environment with no prior preparation. The ability of these techniques to provide selective analyte desorption and ionization in combination with mass spectrometry, has resulted in a growing number of powerful analytical alternatives across broad application areas, both quantitative and qualitative in nature, including pharmaceutical analysis [13], process chemistry [3], biological imaging [4,14], *in vivo* analysis [4,14], proteomics [15], metabolomics [16,17], forensics [10], and explosives detection [18,19].

The important area of ADI-MS was heralded by the innovation of desorption electrospray ionization (DESI) [20] in 2004. Within this rapidly growing field, the leading variants of the developed techniques have shown to be the ones based on plasma desorption and ionization, with many different types of operation and configuration. The most commonly used of these methods is direct analysis in real time (DART) [21], which was established in 2005. Dielectric barrier discharges (DBD), such as dielectric barrier discharge ionization (DBDI) [22] and the low-temperature plasma probe (LTP) [23] are increasingly being used for ADI-MS. They are cheap and easy to construct, which gives them great potential for in-field analysis when coupled to portable mass spectrometers [24]. Such plasmas have proved useful for analytical purposes in many different applications ranging from agrochemicals and food to explosives, personal care products and drugs of abuse. Besides DBDs, other plasma systems generated by rf frequencies have also been utilized for ADI-MS. These include plasma-assisted desorption ionization (PADI) [25] and the atmospheric pressure glow discharge (APGD) [26,27]. Some of these techniques, like PADI, LTP and FA-APGD, have demonstrated a great deal of finesse, in particular for the potential removal of a number of issues often preventing a safe and elegant *in vivo* ambient ionization experiment (e.g. elevated temperature, exposure to high voltages). These techniques rely upon ionization at the

☆ This paper is dedicated to Nicoló Omenetto, on the occasion of his 75th birthday, in recognition of his outstanding contributions to the field of laser spectrochemistry and as an editor of Spectrochimica Acta Part B.

* Corresponding author.
E-mail address: blecic@ifs.hr (V. Horvatic).

http://dx.doi.org/10.1016/j.sab.2014.08.010
0584-8547/

sample surface using a proximate plasma source, rather than a distal plasma such as that used in DART.

A number of optical emission spectroscopy studies [27–35] have been carried out with the aim to determine physical conditions in the ionization sources mentioned above and elucidate the plasma reaction mechanisms by analyzing the components of atmospheric plasmas and their afterglows. For ambient plasmas operating with helium as the discharge gas, it is generally proposed that atmospheric nitrogen, as well as nitrogen impurities in the helium supply [36] play an important role. Ionized nitrogen molecules N_2^+ can be formed by Penning ionization of neutral nitrogen molecules in collisions with helium metastables in the plasma. Another mechanism that is also considered is a cascade of reactions whereby charge is transferred from He_2^+ to atmospheric nitrogen creating N_2^+, which acts as a reagent ion or as a reaction intermediate. In the case of both mechanisms energy transfer to water clusters and then proton transfer to the analyte can then follow. It has been suggested and confirmed [27] that thermal processes which stem directly from the plasma, or from external heating, are needed to desorb analytes from a surface prior to their ionization by plasma species [29].

In the following the most prominent ADI-MS techniques DART, PADI, FA-APGDI and LTP will be outlined, while the recent progress in the field of DBDI, with the focus on DBDs as versatile ionization sources for soft ionization, will be reviewed and analyzed in more detail.

2. Ambient desorption/ionization mass spectrometry techniques

2.1. Direct analysis in real time (DART)

Direct analysis in real time (DART) [21] technology was patented in 2005 and is commercially available. This technique uses a direct-current corona-like discharge, most often sustained in helium, to generate excited species that are then used for desorbing and/or ionizing molecules from a sample. DART has been used to analyze gases, liquids, and solids, but its most prominent feature is the possibility to directly detect chemicals on various surfaces without requiring any sample preparation. This facilitated its widespread application in many different areas. This technique was successfully used for sampling a vast variety of chemicals, including chemical agents and their signatures, pharmaceutics, metabolites, peptides and oligosaccharides, synthetic organics, organometallics, drugs of abuse, explosives, and toxic industrial chemicals. It is suitable for treating thermally unstable samples. The species analyzed by DART are mostly rather small molecules (accessible mass range up to about m/z 1000 [37]). Since DART cannot treat molecules with a large mass, this technique is somewhat inconvenient for biomolecular sample analysis such as proteomics and glycomics. Recent reviews on DART technique have been given by Chernetsova et al. [38] and Gross [39].

A schematic illustration of DART technique is shown in Fig. 1. DART [21] is based upon the formation of a plasma discharge in a gas (nitrogen or helium) which flows through several chambers (Fig. 1). In the second chamber a pair of perforated electrodes is located which can be biased to remove ions from the gas stream. Thus, in DART the charged plasma species are filtered so that eventually only the metastable atoms can reach ambient air. In the third chamber the stream of metastable atoms can be optionally heated (up to 823 K) to enhance the thermal desorption.

One of the ionization mechanisms in DART has been attributed to possible Penning ionization. It involves energy transfer from the gas atom excited to the metastable state M* to an analyte S having an ionization potential lower than the energy of M*, producing a radical molecular cation of the analyte. Penning ionization is a dominant reaction mechanism when nitrogen or neon is used in DART source. If helium is used, ionization mechanism involves the formation of ionized water clusters in reaction of metastable He atoms and atmospheric water. This is followed by proton transfer from ionized water clusters to the analyte and formation of protonated analyte molecule. Analyte ions are eventually sampled by the mass spectrometer.

2.2. Plasma assisted desorption/ionization (PADI)

The PADI technique was introduced in 2007 by Ratcliffe et al. [25]. It is based on generating a non-thermal radio-frequency glow discharge, which is allowed to interact with the sample surface as illustrated in Fig. 2. The discharge burns between a pin electrode and the sample or the mass spectrometer inlet, which serves as the counter electrode.

The interaction of the plasma with the sample surface results with desorption and ionization of the target analyte material and the created ions are readily detected with a suitable mass spectrometer. The plasma plume of PADI is a "cold" one with an operating temperature close to that of the ambient environment, which is particularly useful for thermally sensitive samples. This method when coupled with atmospheric pressure sampling mass spectrometry yields mass spectral information under ambient conditions of pressure and humidity from various surfaces without the requirement for sample preparation or additives.

The potential of PADI has been demonstrated for the rapid analysis of pharmaceuticals. Results [25] have shown the effectiveness of the method for generating high-quality data from various pharmaceutical formulations, such as tablets and creams, suggesting that the methodology is promising for future applications.

2.3. Flowing afterglow-atmospheric pressure glow discharge ionization (FA-APGDI)

Flowing afterglow-atmospheric pressure glow discharge (FA-APGD) – also known as flowing atmospheric pressure afterglow (FAPA) – is a plasma-based technique that utilizes the afterglow to ionize the analyte in the ambient air region between the plasma source and the mass spectrometer, instead of the plasma directly interacting with the sample (see Fig. 3).

FA-APGDI was introduced in 2008 by Andrade et al. [40] for studying gaseous samples and for the direct desorption/ionization mass spectrometric analysis of different analytes from solid substrates [41]. The ionization source is capable of ionizing both polar and nonpolar substances to be detected by mass spectrometry, and to perform spatially resolved analysis of the sample [41]. This technique enables direct analysis of liquid and solid (soluble or insoluble) bulk polymers and granulates, while the introduction of the samples to the gas stream outside the discharge chamber overcomes problems of discharge instability and memory effects, and at the same time allows rapid, high-throughput analyses

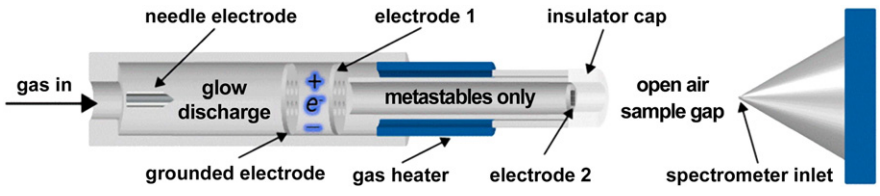

Fig. 1. Schematic illustration of DART technique.

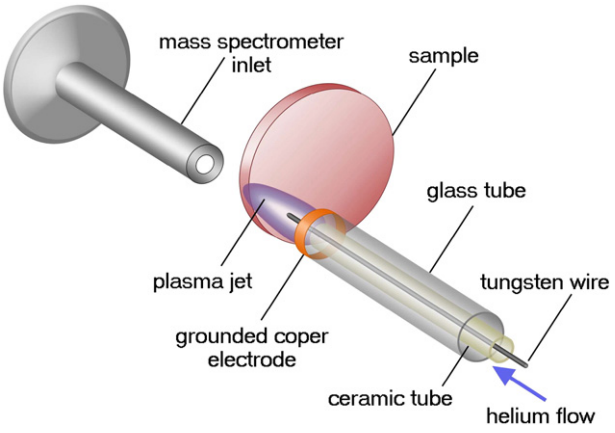

Fig. 2. Schematic illustration of PADI technique.

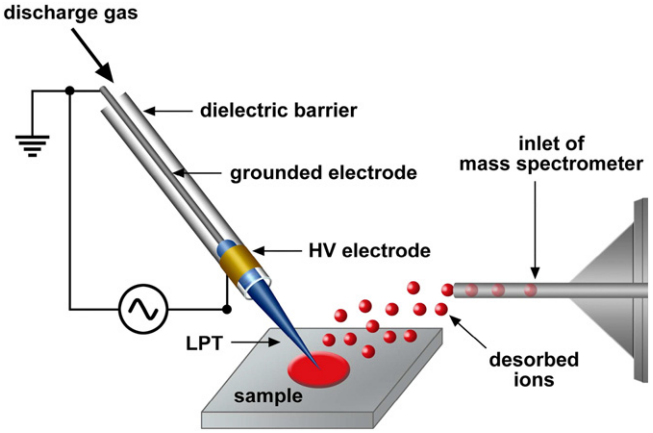

Fig. 4. Schematic illustration of LTP probe.

[40–42]. Recently, with this technique the analysis of pesticides in fruit peel and fruit juices by direct detection has been performed successfully [42].

The use of unfiltered afterglow is advantageous for the ionization of lower polarity analytes, but on the other side makes mass spectra more complicated due to increased number of background ions and different adduct species [43]. A major limitation of this technique is the inability to thermally desorb larger molecules (accessible mass range $m/z < 500$ [44]), which makes it unsuitable for molecular weight determination and differentiation of polydispersed polymers [44,45].

2.4. Low-temperature plasma probe (LTP)

A recently disclosed plasma-based method showing increasing applicability is the low temperature plasma (LTP) probe [23]. In this technique (see illustration in Fig. 4) the alternating-current plasma is generated in a probe configuration, which enables increased flexibility and non-proximate analysis of bulk samples or large objects.

In most cases where plasma ionization is employed, the sample is placed close to or within the discharge area for ionization, which constitutes the physical restriction. The design of the LTP probe allows the plasma species to be extracted by the combined action of the gas flow and the electric field, with a torch extending beyond the glass tube, which is suitable for direct surface sampling. The temperature of the sample area in contact with the plasma torch was measured to be about 30 °C, so no damage to the surface due to heating is expected, thus making this technique appropriate for treating thermally sensitive samples. The following advantageous performance characteristics of the method were demonstrated [23]: positive or negative ions can be produced from a wide range of chemical compounds in the pure state and as mixtures in gases, solutions, or condensed phases, using He as the discharge gas. A limited fragmentation is present and it can be easily controlled by the adjustment of the electrode configuration during operation. A wide range of the applicability of the technique was demonstrated by direct analysis of cocaine from human skin, determination of active ingredients directly in drug tablets, and analysis of toxic and therapeutic compounds in complex biological samples.

2.5. Dielectric barrier discharge ionization (DBDI)

The first DBDI source for ambient mass spectroscopy was developed by Na et al. [22] in 2007. It was based on a dielectric barrier discharge formed between a copper sheet electrode and a metal needle electrode, as illustrated in Fig. 5. A glass plate situated between electrodes served as dielectric barrier as well as sample plate.

With an alternating voltage applied between the electrodes, a stable low-temperature plasma was formed between the tip of the discharge

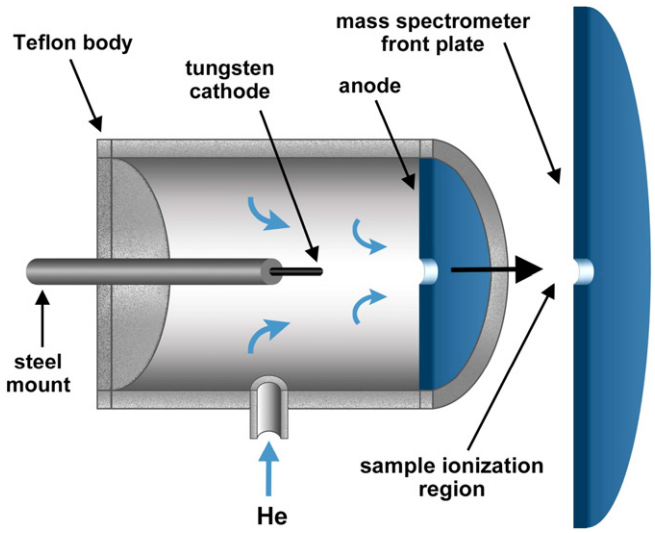

Fig. 3. Schematic illustration of FA-APGDI technique. The blue arrows indicate the He flow.

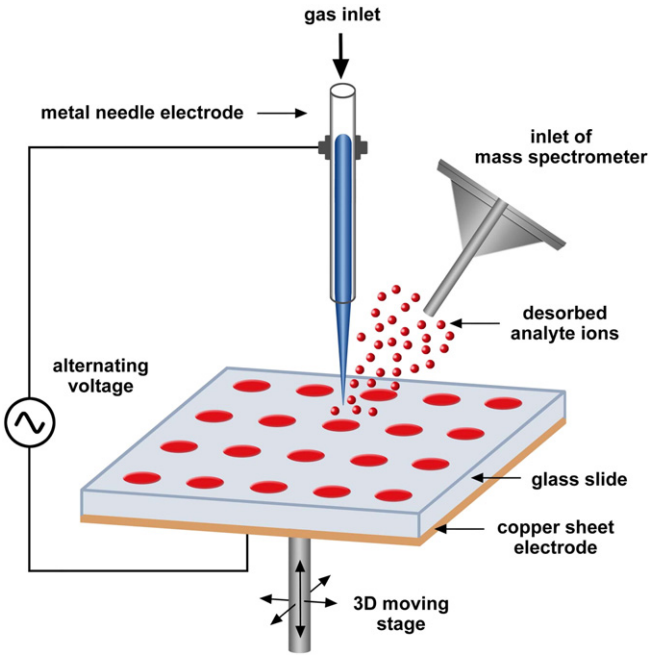

Fig. 5. Schematic illustration of DBDI technique.

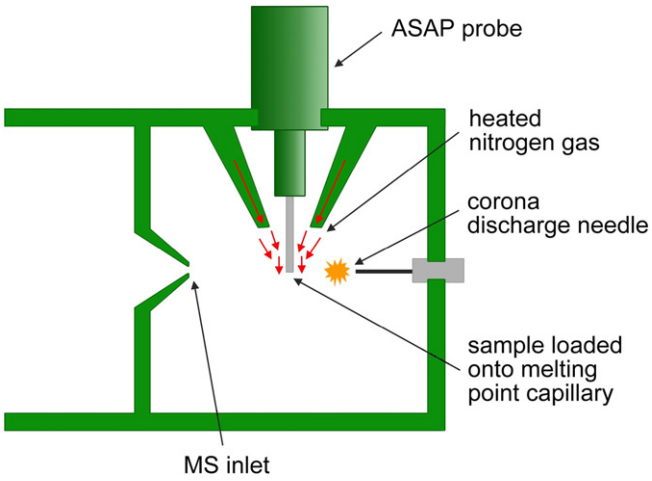

Fig. 6. Schematic illustration of ASAP technique.

electrode and the surface of glass slide, which was used to desorb and ionize analytes deposited on the glass surface. Eventually the produced ions were introduced to the mass spectrometer for mass analysis.

The designed DBDI source has the advantage of being small in size and having simple configuration. It is appropriate for imaging of biological samples since the needle-plate discharge can be localized within an area of several micrometers. Its potential was demonstrated by the analysis of twenty amino acids separately deposited on a glass slide, which were analyzed individually.

2.6. Atmospheric solids analysis probe (ASAP)

The atmospheric solids analysis probe (ASAP) (Fig. 6), introduced by McEwen et al. [46], is a useful tool for the rapid direct analysis of volatile and semi-volatile, solid and liquid samples under atmospheric pressure ionization (API) conditions. Vaporization of the sample from a disposable glass capillary tip is achieved with a hot nitrogen gas stream. The sample is then ionized with the in-situ corona discharge pin. This allows

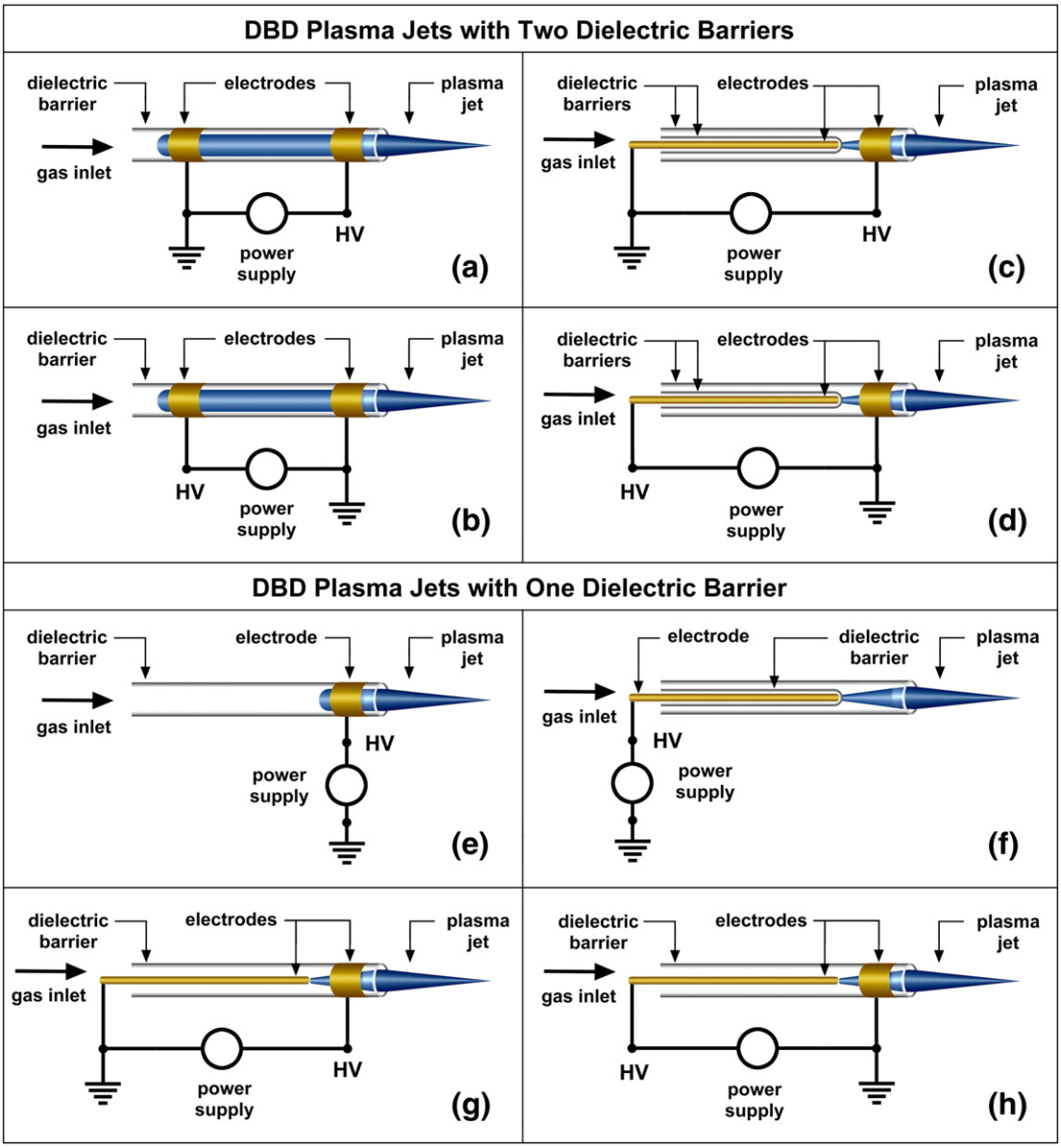

Fig. 7. Different DBD plasma jet configurations.

low polarity compounds to be ionized with a high degree of sensitivity. Furthermore, complex mixtures can be analyzed without the need for any sample preparation.

3. Dielectric barrier discharge ionization sources for soft ionization

3.1. Different configurations of DBDI sources

Capillary dielectric barrier discharges producing plasma jets that extend in the surrounding atmosphere are versatile, cheap and easy to construct devices that have found extensive use as ionization sources in the ambient desorption/ionization mass spectrometry techniques. There are various designs of the construction of DBD ionization sources. In Fig. 7 different configurations for a plasma jet with one or two dielectric barriers are depicted.

Fig. 7a and b shows DBD with two dielectric barriers, consisting of a dielectric tube with two metal ring electrodes on the outer side of the tube. This configuration was first reported by Teschke et al. [47]. When a working gas (He, Ar) flows through the dielectric tube and a kHz high-voltage is applied to the electrodes, a cold plasma jet is generated in the ambient air. The plasma jet only consumes a power of several watts. The gas temperature of the plasma is close to room temperature.

One of the high-voltage ring electrodes can be replaced with a centered pin electrode inside the glass capillary, which is covered with a dielectric [48], as depicted in Fig. 7c and d. Such design enhances the electric field along the plasma jet. A high electric field along the plasma jet is favorable for generating long plasma plumes and more active plasma chemistry [49].

Configurations of DBD with one dielectric barrier are shown in Fig. 7e–h. A pin electrode centered in the capillary can be electrically grounded (Fig. 7g) or supplied with high-voltage (Fig. 7h). These devices can be driven by kHz ac power, by rf power or by pulsed dc power.

The DBD with one dielectric barrier and one ring electrode, as reported in [50], is illustrated in Fig. 7e. Such construction results with weakening of the discharge inside the dielectric tube.

Another variant DBD of this configuration in which the ring electrode is altogether removed [51] is shown in Fig. 7f. This configuration also weakens the discharge in the capillary.

In all the described cases the discharge inside the capillary as well as the plasma jet outside the capillary can be influenced by an electrically conducting material, which is brought in contact with the plasma jet. In the case shown in Fig. 7h there will be a drastic change when a metallic object or an electrical ground is targeted with plasma jet. For such a circumstance, the discharge will no longer operate as a DBD, i.e. it will transform to direct discharge with much higher current and therefore higher power.

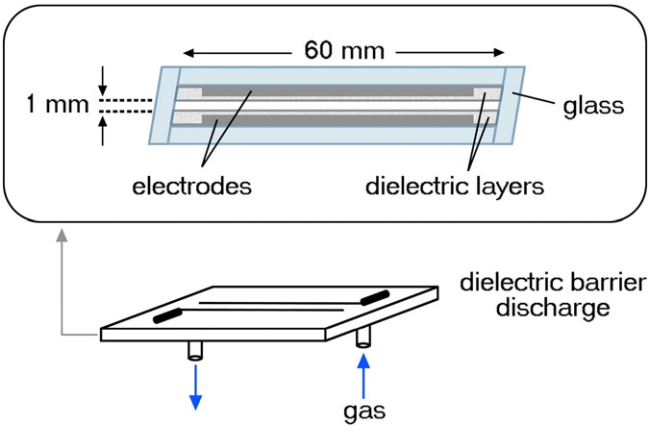

Fig. 8. The design of the miniature planar DBD microchip source for analytical purposes as reported in [52].

3.2. The outset of DBD use for analytical spectrometry

In 2001, several years before the DBDI technique for ADI-MS was established by Na et al. [22], the potential of dielectric barrier discharge plasma for analytical element spectrometry was demonstrated by the work of Miclea et al. [52]. The authors presented a miniature planar DBD (Fig. 8), characterized by small size, low power consumption, low gas temperature and excellent dissociation capability for molecular species. The DBD showed excellent analytical results in the plasma modulation diode laser atomic absorption spectrometry (DLAAS) of halogenated hydrocarbons in noble gases as well as in air/noble gas mixtures, with the analytical figures of merit comparable with the results found earlier with dc [53,54] and microwave induced plasmas [55] of larger size with much higher plasma powers.

Just coinciding with [22], another work [56] was published that reported a miniaturized excitation source for ambient soft ionization of molecules based on a dielectric barrier discharge. Fig. 9 shows a photograph of the dielectric barrier discharge with a plasma jet extending to ambient atmosphere equivalent to the one used in [56]. The discharge was produced in a 3 cm long glass capillary with an inner diameter of 500 μm and an outer diameter of 1.2 mm. The electrodes, separated by 12 mm, were formed of 500 μm thick silver wire. The distance of the electrode to the capillary orifice was 2 mm. The discharge was running in helium (purity: 99.999%, with 3 ppm of N_2 impurity) and was sustained by applying positive pulses from an ac generator.

This miniaturized plasma was proposed to be used for the ionization of gaseous compounds under atmospheric pressure as an alternative to traditional atmospheric pressure chemical ionization (APCI). It was applied as ionization source for ion mobility spectrometry where the common sources are radioactive, thus limiting the place of installation. The comparison of plasma IMS with β-radiation IMS [57] was made. It was shown that the plasma IMS had approximately two orders of magnitude higher sensitivity and greater selectivity than the β-radiation IMS.

The authors in [56] were the first to investigate the fundamental processes occurring in DBD plasma that play crucial role in ambient soft ionization methods. Spatially resolved spectroscopic measurements were carried out in order to investigate mechanism of the production of N_2^+ outside the capillary, which is relevant for the protonation of analyte molecules and sustains the production of primary ions. It was argued here that the excited noble gas atoms and the nitrogen ions are responsible for the soft ionization of the analyte.

3.3. Ionization mechanisms in helium DBDI sources

Several papers [28,29,33] have been published recently on the investigation of the underlying processes in helium dielectric barrier discharges used for soft ionization. These processes in the cascade of reactions lead to a formation of protonated water molecules, which are needed to ionize analytes. It is commonly agreed that the starting point in this chain of reactions is the formation of ionized nitrogen molecules N_2^+. Two reaction channels are being considered as likely

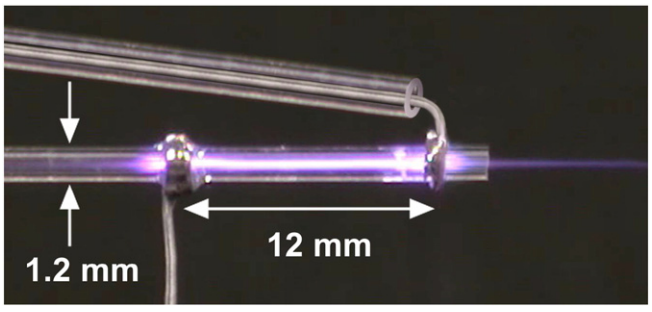

Fig. 9. The photograph of the helium capillary DBD with a plasma jet extending in the open air, equivalent to that used in [56] as ionization source for ambient soft ionization.

candidates for the N_2^+ formation. The first is Penning ionization of nitrogen in collisions with helium metastables:

$$He^M + N_2\left(X^1\Sigma_g^+\right) \rightarrow N_2^+\left(B^2\Sigma_u^+\right) + He + e^- + \Delta E_1 \quad (1)$$

and the second one is the charge transfer occurring in collisions of ionized helium with neutral nitrogen molecules:

$$He_2^+\left(X^2\Sigma_g^+\right) + N_2\left(X^1\Sigma_g^+\right) \rightarrow N_2^+\left(B^2\Sigma_u^+\right) + 2He + \Delta E_2 \quad (2)$$

Optical emission spectroscopy was used [28,29,33] to determine spatial distributions and rotational temperatures of the relevant species (He*, O, N_2^+, N_2, H, OH) in the plasma and in the jet with the aim of finding out which of the above reactions governs, and is more favorable for the efficiency of the soft ionization, but an unambiguous answer has not been given yet.

In the following, the recent progress in this segment of understanding of the basic processes in DBSs intended for use as soft ionization sources will be reviewed.

3.3.1. Spatial distributions of relevant species in helium DBDI sources

For many analytical applications especially for desorption and ionization a plasma jet with a pin electrode and one ring electrode as described by Chan et al. [28] was used. Here one dielectric barrier is between the electrodes. A characterization of the plasma jet in respect on the maxima of He*, O, N_2^+, N_2, H and OH has been presented.

Fig. 10 shows the partial energy diagram of He. It will be helpful for the discussion of the results presented here.

Fig. 11 is taken and modified from [28] and shows normalized vertical emission profiles of selected atomic and molecular species in the He-LTP. The emission profiles of H_α 656.3 nm and OH 308 nm shown in the original graph are not plotted. The zero position refers to the end of the capillary, with positive positions extending outside the torch into the open atmosphere. The authors made a few interesting observations.

The first described observation was that the maximum emission for He (the plasma gas) and O, occurred inside the torch, whereas the maximum emission for both N_2^+ and N_2 appeared in the open atmosphere. The second observation shows that the shapes of the emission profiles for N_2^+ and N_2 were similar but spatially shifted, with the maximum in N_2 occurring farther downstream from the end of the torch than N_2^+.

Additionally, little N_2 emission was detected within the plasma torch, except near the edge open to atmosphere, whereas significant N_2^+ was observed for all measured regions inside the plasma torch. Because the emission of both nitrogen molecular species decayed from the torch edge inwards, the authors believe that nitrogen species observed in these emission studies, result from atmospheric nitrogen diffusing into the ionization source rather than from impurities in the gas supply. Nevertheless, it is surprising that N_2 emission signal is practically zero in the region −6 to −2, while the intensity of N_2^+ is still quite high. This effect needs to be further examined, preferably with time resolved measurements.

The third observation of the authors was that 4.5 mm outside the plasma torch, a local maximum existed for He emission that directly coincides with the peak emission of N_2^+. One might see this as a second maximum but it could also be interpreted that there is a minimum (dip) in between two maxima. A comparison of the He and the O vertical emission profile shows that both signals have a similar increase between position −6 and −2 up to the maximum and between position 6 and 13. The decay of the He signal between positions −2 and 2 is much faster than the decay of the O signal. When having an atmosphere without N_2 but with pure He the spatial behavior of He would be similar to the course of O. Apart from the extent of excited He atoms, which might be longer than in the air surrounding there will be no minimum measurable. We have fitted the measured points of the He 706 nm line to extreme function (one of the Origin built-in functions) which exhibits maximum followed by monotonous decrease. In this fit only the data in the range from −6 to −3 and from 5 to 13 were used, i.e. the region where the He signal has a minimum was excluded. The measured data of the He 706 nm line were then subtracted from the fit. The obtained difference is presented in Fig. 11 with blue symbols and could represent a value which might be proportional to the density of the He^M. The idea behind this procedure is that the He 706 nm line corresponds to the transition from excited 3s ^3S state to lower-lying 2p $^3P_J^o$ state, which radiatively decays to 2s $^3S_1$ metastable state (see Fig. 10). Thus, the decrease in the population of 3s ^3S state, reflected in the decrease of 706 nm line intensity, eventually leads to the accumulation of the population in the lowest lying metastable state. In other words, the 706 nm line intensity decrease is proportional to the increase of metastable density.

This strengthens the fourth observation of the authors, that the emission of both N_2^+ and N_2 attained their maxima around 5 mm and 8 mm, respectively, outside the plasma torch. It is plausible to deduce

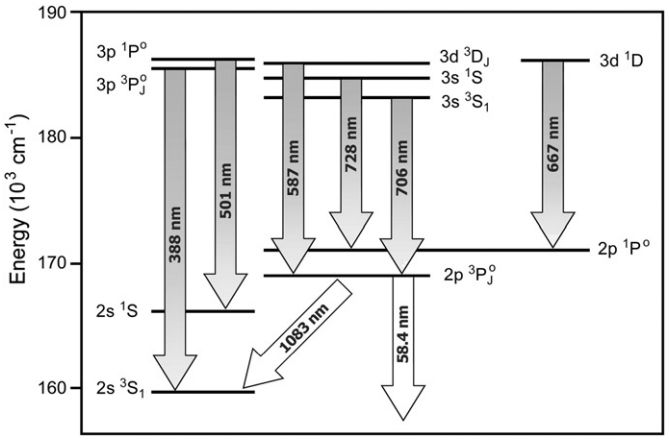

Fig. 10. The partial energy diagram of helium is composed of the lowest lying excited states. Shaded arrows indicate the transitions considered here. In addition, the resonance line at 58.4 nm and the transition at 1083 nm are represented by hollow arrows.

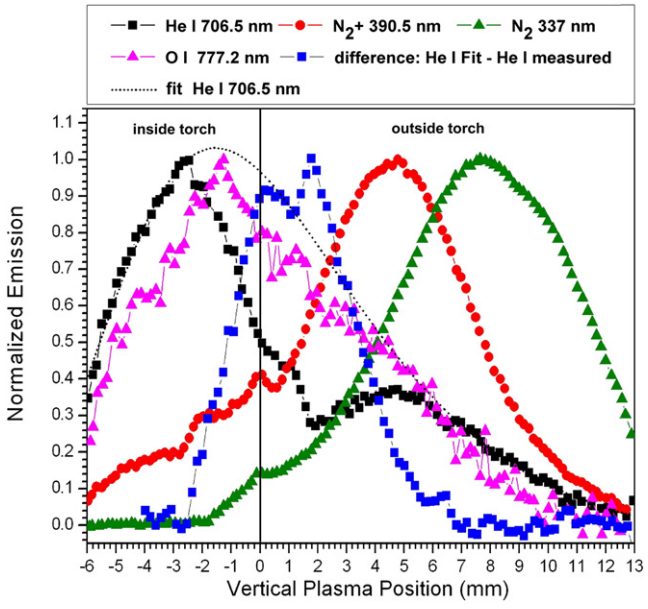

Fig. 11. Normalized vertical emission profiles of He I 706.5 nm, O 777.2 nm, N_2^+ 390.5 nm and the N_2 337 nm obtained in the He-LTP. Position zero is the edge of the glass torch with positive values extending into the ambient atmosphere. The results are digitized from Fig. 3 in Ref. [28] and the difference signal (see text for the details) between fitted (dotted curve) and measured He I signals is added (blue symbols).

that in this spatial region the dominant mechanism of excitation of both species is not through electron impact. The spatial shift of N_2 emission relative to that of N_2^+ implies that the excited N_2 molecules might be formed via recombination of N_2^+ with an electron. Likely mechanisms for the formation of N_2^+ are given by Eqs. (1) and (2). The common belief is that in the region outside the torch electron impact processes will primarily excite lower excited He* and He^M metastable states. Therefore, the reaction cannel in Eq. (2) should be far less efficient for the N_2^+ creation than the Penning ionization process described with Eq. (1).

The difference signal between the fitted and measured He 706 nm data shown in Fig. 11, exhibits maximum around position 2 that just precedes the steeper raise of the N_2^+ signal. If we adopt the interpretation that this signal might be a measure for the maximum of the He^M population then Fig. 11 shows that it is just at the right location to initiate N_2^+ formation by the process (1). This interpretation would satisfactorily explain the spatial sequence of the signals displayed in Fig. 11 and would be in good agreement with the theory that in the open atmosphere region electrons will mainly excite lower excited He* and metastable He^M states. Excited He* atoms will then radiatively decay into He^M, which by Penning ionization process (1) form N_2^+, and eventually the excited N_2 molecules are formed by electron recombination of N_2^+.

The investigation similar to [28], but for helium DBD in the configuration with two ring electrodes around the capillary tube was reported by Müller et al. [33]. Optical emission spectroscopy was used to determine spatial distributions of the excited helium atoms He* as well as ionized and neutral nitrogen molecules, N_2^+ and N_2, respectively. The measurements were done in the capillary and in the jet. The dependence of the spatial distributions on the voltage applied on DBD and helium flow was examined. A representative of the performed investigations is reproduced from [33] and displayed in Fig. 12. Helium emission line at 388 nm (transition from the 3p $^3P_J^o$ state to the lowest metastable 2s ^3S_J state) was used to inspect the behavior of the excited state helium population, while the intensities of the heads of the N_2^+ 391 nm and N_2 380 nm bands were measured to determine distributions of N_2^+ and N_2 molecules. The results obtained with working voltage of 3.8 kV and a constant He flow of 500 ml/min are shown in Fig. 12. Regarding the positions of the maxima of He*, N_2^+ and N_2 signals, the observed intensity distributions are in good agreement with the observations reported in [28]. The emission of He* (388 nm line) exhibits the maximum inside the capillary, followed by the decrease which reaches a minimum (dip) at the position −1.5 mm (inside the capillary). A mild increase than occurs in the jet region up to distances of ~+2 mm, after which the signal eventually extinguishes. Maximum emissions of N_2^+ and N_2 appear in the plasma jet, here at positions 2 and 3.5 mm, respectively, which is also in agreement with the behavior in the plasma jet with the pin electrode centered in the capillary [28].

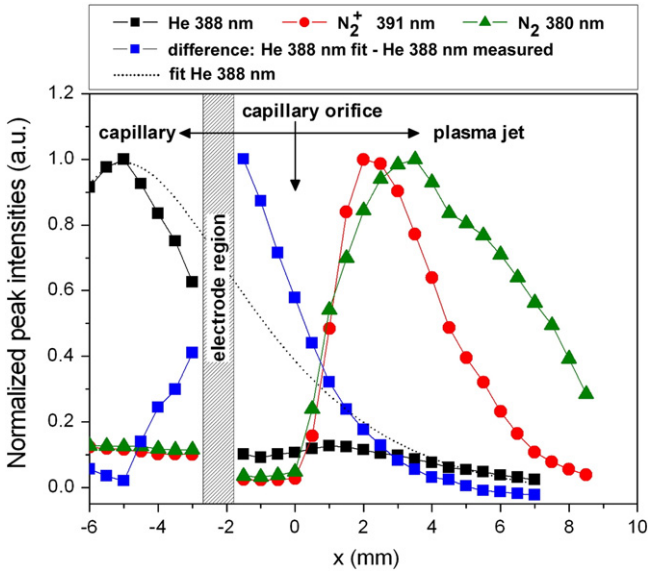

Fig. 12. Normalized spatial distributions of the excited helium atoms and ionized and neutral nitrogen molecules observed in capillary helium DBD with two-electrode and two dielectric layers geometry. The experimental points are taken from Ref. [33] and normalized for the purpose of the current presentation. The fit of the He 388 nm emission intensities to a function exhibiting only one extreme is depicted with dotted line.

In addition to 388 nm line, spatial distributions of five more He lines (501, 587, 667, 706 and 728 nm) were investigated in [33]. These lines correspond to the transitions from higher excited states to either 2p $^1P_1^o$ resonance state or the lower-lying 2p $^3P_J^o$ as well as the metastable 2s $^1S_0$ and the 2s $^3S_1$ states (see Fig. 10). They all exhibited characteristic dip in spatial distribution similar to one observed for the 388 nm line (Fig. 12). It is worth noting that the populations in the upper states of all mentioned lines eventually relax to the metastable states, either directly or through the cascade of radiative or collisional transitions involving resonance 2p $^1P_1^o$ and lower-lying 2p $^3P_J^o$ state.

If the minimum in the He 388 nm intensity distribution is again treated to be due to relaxation of He* into He^M, as done above for the results of Chan et al. [28], the maximum can be estimated as follows. The truncated set of He 388 nm data, composed of the points at positions between −6 and −3 mm, and between position 4 and 7 mm was fitted to a function that monotonously decreases after exhibiting extreme (Origin Extreme function). The fit is depicted with a dotted line in Fig. 12. The measured He 388 nm data were subtracted from the fitted values and the difference signal, which might be representative for the population of metastable He^M atoms, is shown in Fig. 12 with blue symbols. It is in qualitative agreement with the analogous difference signal obtained for the plasma jet with pin electrode shown in Fig. 11. The discussion made above in relation to interpretation of this difference signal is applicable here as well.

When the applied DBD voltage is increased from 3.8 kV to 4.5 kV the shape of the peak line intensity distributions of the He 388 nm line and the intensity distributions of the heads of the N_2^+ 391 nm and N_2 380 nm bands changed. Not only the maxima of N_2^+ and N_2 nearly overlapped but also the minimum of the He 388 nm line distribution was shifted away from the capillary outlet close to the maxima of the N_2^+ and N_2. These differences were related to the change of the DBD working regime from homogeneous to filamentary (Section 3.3.2.), which can be induced by increasing high voltage above a certain threshold.

3.3.2. Operation modes of helium capillary DBD

Recently it has been found [33] that the operation mode of a capillary DBD running in helium can be easily switched between homogeneous and filamentary just by changing the operating voltage of the DBD.

The DBD reported in [33] consisted of a 30 mm long glass capillary (outer diameter: 1 mm, inner diameter: 500 μm), with two electrodes surrounding the capillary. One end of the capillary served as gas inlet and the other one is left in open air. The electrodes were 1 mm wide and separated by 10 mm. High voltage was applied to the electrodes to sustain the discharge, which generated the plasma jet in the ambient air. The stable plasma operation was obtainable for the voltages in the range between 3.5 and 6.5 kV (voltage amplitude) at 21.5 kHz.

For the working voltages up to 4 kV, a single current peak was recorded, which represents the plasma ignition (encircled signal in Fig. 13a). The width of the peak was less than 2 μs (cannot be discerned in the figure) and corresponds to the time when the plasma is on.

At voltages higher than 4 kV, the initial current signal was followed by a series of short consecutive peaks resembling beats (encircled signal in Fig. 13b). The time span of the beats depended on the applied voltage, and was between 5 and 7 μs for the voltages in the range from 4.5 and 6.5 kV, respectively.

According to Wagner et al. [58] a sharp single peak in the DBD current indicates that the plasma operates in a homogeneous mode, while a series of short consecutive current peaks is a characteristic of a

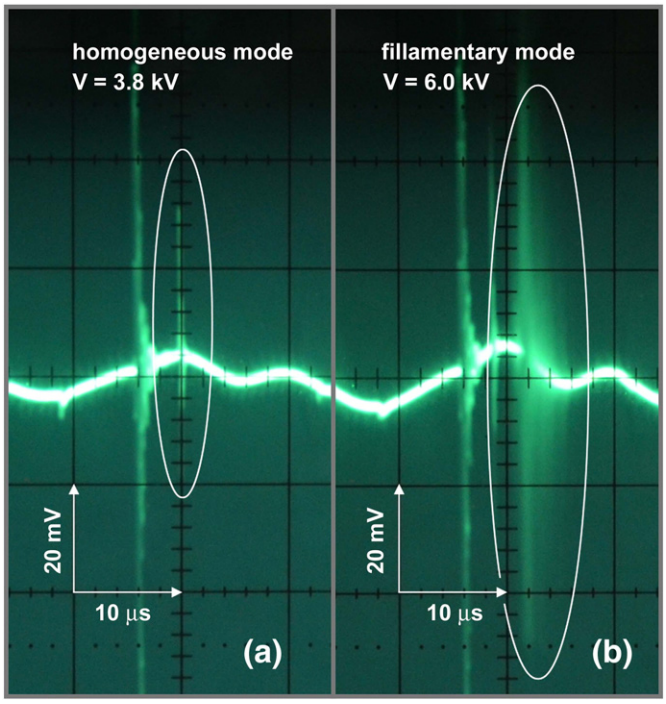

Fig. 13. Oscilloscope traces of the DBD current signals [33] recorded in homogeneous (a) and filamentary (b) DBD operation modes. Encircled signals correspond to the DBD current. Strong spikes to the left of the current signals are due to coupling of the function generator and the high-voltage plasma generator to the oscilloscope input.

filamentary operation mode. Therefore, the authors in [33] concluded that the investigated DBD was running in the homogeneous mode at voltages below 4 kV, while at higher voltages, for most of the time, it worked in the filamentary mode.

3.3.3. Rotational temperatures of N_2^+ in helium capillary DBD

It has been shown by Endoh et al. [59] that the rotational energy distribution of the N_2^+ species strongly depends on the ionization pathway, i.e. reaction channel through which they are formed. Penning ionization of N_2 by He^M (Eq. (1)) and charge transfer from He_2^+ (Eq. (2)) at thermal energies were studied by monitoring emission from different rotational N_2^+ levels and the rotational temperatures for both reactions were determined from the corresponding Boltzmann plots. The rotational temperatures of N_2^+ originating from Penning ionization and charge transfer differed considerably, and amounted to 360 and 900 K, respectively.

Spatial distribution of rotational temperatures of the N_2^+ molecule in the capillary helium DBD with two ring electrodes was investigated by [33] using the line intensities of the N_2^+ band with maximum at 391 nm. Rotational temperatures were determined in both homogeneous and filamentary DBD operation mode (Fig. 14a). In the homogeneous mode, the rotational temperatures remain practically constant in the capillary as well as in the jet (~40 K above the room temperature). In the filamentary mode, rotational temperatures increase when approaching the anode region and their values saturate in the jet at about 410 K.

The study of spatially resolved rotational temperatures in the helium LTP DBD with pin electrode centered to the capillary, based on the measurements of OH and N_2^+ molecular emission bands at 308 and 391 nm, respectively, was reported by Chan et al. [28,29]. The results reproduced from [29] are presented in Fig. 14b. It was found that both inside and outside the torch the rotational temperatures of the OH molecules were very similar to room temperature and agreed well with values obtained by infrared thermometry. However, rotational temperatures of N_2^+ were found to be much higher, reaching as much as 550 K outside the torch without exhibiting saturation. The authors explained that the reason for the discrepancy in the OH and N_2^+ rotational temperatures was due to additional rotational energy imparted to the N_2^+ molecule during the ionization process. Based on the observed N_2^+ rotational-energy distribution the authors [29] deduced that a significant fraction of N_2 was ionized by charge transfer reaction given by Eq. (2). This finding was contrary to most previously published investigations [21,23,25], which solely assumed a Penning ionization process (Eq. (1)).

There is a common assumption that a rapid equilibrium exists between rotational levels and translation energies of a molecule in atmospheric-pressure plasma. The results in [29] showed that this, different to the case of OH molecules, was not fulfilled for N_2^+ ions. Thus, the authors concluded that rotational temperatures of N_2^+ in helium based plasmas are not a reliable measure of gas temperatures but rather an indicator of the of N_2^+ reaction channel production.

When comparing N_2^+ rotational temperatures in Fig. 14a and b it is easily seen that the data of [33] obtained in the filamentary mode resemble the result of [29]. In both cases the rotational temperatures start to increase near the capillary orifice and continue to rise in the

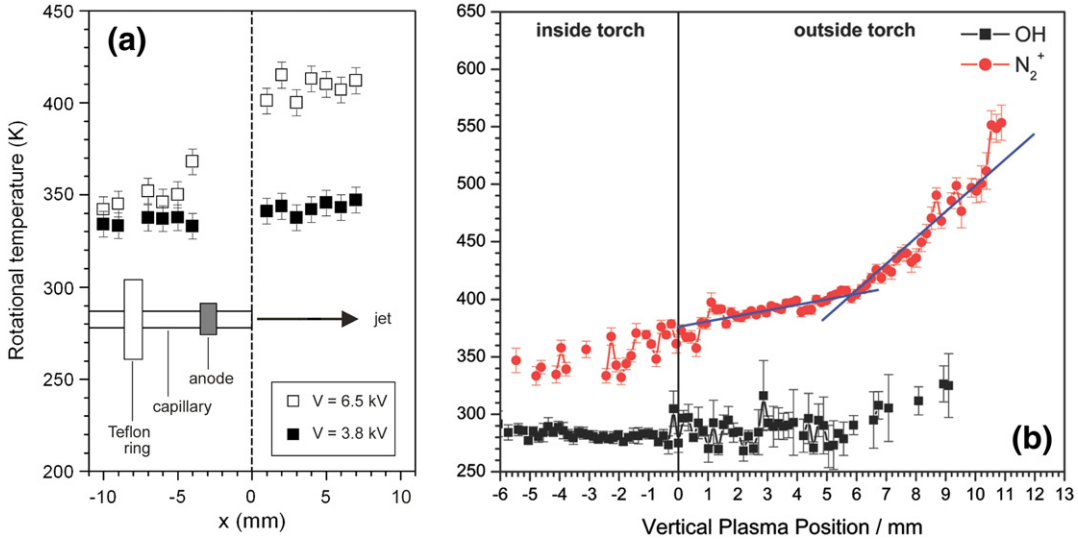

Fig. 14. (a) Spatial distribution of rotational temperatures of the N_2^+ molecule in the capillary helium DBD with two ring electrodes (reproduced from [33]). Black symbols: homogeneous operation mode, open symbols: filamentary operation mode. (b) Spatially resolved rotational temperatures of OH and N_2^+ in the helium LTP DBD with pin electrode centered to the capillary. The results are reproduced from [29].

ambient atmosphere reaching comparable values. The only difference regards the existence of the saturation plateau in the region farthest from the capillary end, which is not present in the data from [29].

The conditions of the DBD plasma jet in [33] and the LTP pin electrode plasma [29] are certainly different. The differences are due to the discharge tube geometry, the electrode design, and the gas velocities, which in the case of the DBD plasma jet are about one order of magnitude higher. However, on the basis of the rotational temperature data, one can conclude that in the DBD plasma jet [33] working in filamentary mode and in the case of the LTP pin electrode plasma [29] the charge transfer reaction (2) in the plasma jet plays a significant role.

According to the results discussed above it can be concluded that DBD running in filamentary mode (high applied voltages) produces "hot" (400–500 K) N_2^+ ions in the plasma jet. Most likely both reactions (1) and (2) contribute to N_2^+ creation in these conditions, but the elevation of the rotational temperatures above the room temperature should be ascribed to N_2^+ ions stemming from charge transfer reaction (2). On the other hand, DBD working at lower voltages, i.e. in the homogeneous mode, produces "cold" (close to room temperature) N_2^+ ions in the plasma jet whose major production should be attributed to the Penning ionization process (1).

The impact of homogeneous and filamentary DBD modes on the efficiency of dielectric barrier discharge ionization mass spectrometry was previously checked by Meyer et al. [60]. The experiment was performed by laser desorption-DBDI-mass spectrometry (LD-DBDI-MS). A diode laser was used to desorb the solid analyte substance deposited on a glass surface. The desorbed neutral molecules were then ionized by the DBDI source and subsequently transported into the inlet of the mass spectrometer. It was found that LD-DBDI-MS intensities of the protonated parent ions $[M + H]^+$ of propazine obtained using helium DBDI operating in homogeneous mode were about three times higher than in filamentary mode.

Recently, the ionization efficiency of the DBD against the operation modes has been checked on an analyte different to the one investigated by [60], using different sample preparation method. The capillary helium DBD analogous to the one reported by [33] was supplied with sinusoidal high voltage of variable amplitude (up to 4 kV) at 20 kHz. The formed jet was used to ionize Tryptophan (10 mM, m/z 205.1) in methanol and H_2O (50:50 vv). The sample was introduced into the ionization source in front of the MS by a thermospray where the analyte was applied continuously. The mass spectrometer signal obtained varying the voltage across homogeneous and filamentary mode is shown in Fig. 15. As can be seen, the maximum MS signal is measured at 3 kV, i.e., at the highest voltage at which the DBD still operated in homogeneous mode. The maximum MS signal was more than two orders of magnitude higher than in filamentary mode, indicating that the homogeneous mode is much more appropriate for achieving efficient ionization of the analyte. Compared with the results in [60] the more pronounced efficiency difference observed here can be attributed to different methods of target preparation (laser desorption [60] and thermospray).

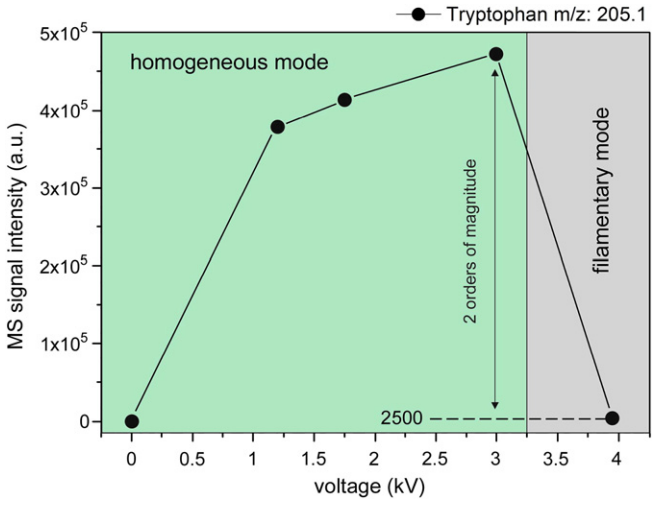

Fig. 15. Mass spectrometer signal of Tryptophan (10 mM, m/z 205.1) in methanol and H_2O (50:50 vv) obtained with capillary DBD ionization source operated in homogeneous and filamentary mode.

4. Conclusion

The methods developed for ambient desorption/ionization mass spectrometry (ADI-MS) are briefly outlined. The emphasis has been put on recent advances in the development and understanding of helium dielectric barrier discharges used as sources for soft ionization of molecules. Basic mechanisms for the formation of protonated water required for the soft ionization of analytes have been considered. They all involve formation of ionized nitrogen molecules N_2^+ as a starting point for the subsequent cascade of reactions with water molecules that eventually generate protonated water. In He DBD N_2^+ molecules can be formed through two reaction channels: by Penning ionization of N_2 in collisions with helium metastable atoms He^M, or by charge transfer from He_2^+ ions in collisions with ground state nitrogen molecules N_2. The characteristic of the N_2^+ created by Penning ionization is that their rotational temperatures are low, close to room temperature, while the rotational temperatures of N_2^+ resulting from charge transfer can reach as much as 900 K.

Recent investigations have shown that the working regime of the helium DBD can be changed from homogeneous to filamentary by increasing the applied voltage above certain threshold value. The two operation modes are characterized with very different rotational temperatures of N_2^+ ions present in DBD jet. In the homogeneous mode (low operating voltages) the generated N_2^+ species are "cold", having rotational temperatures close to room temperature, while in the filamentary mode (high operating voltages) "hot" N_2^+ are produced whose temperatures can be as high as 500 K. Consequently, it can be concluded that in a DBD running in homogeneous mode N_2^+ ions are the result of Penning ionization process, while in the filamentary mode N_2^+ are formed preferably by charge transfer reaction. The ultimate question – what is better for efficient soft ionization – has been tried to answer recently by performing mass spectrometry of Tryptophan molecule using capillary helium DBD as ionization source. It turned out that homogeneous mode performed better, because the observed MS signals were more than two orders of magnitude higher than in filamentary mode.

Acknowledgments

The financial support by the Ministerium für Innovation, Wissenschaft und Forschung des Landes Nordrhein-Westfalen, the Bundesministerium für Bildung und Forschung, the Deutsche Forschungsgemeinschaft (project No. FR 1192/13-1) is gratefully acknowledged.

This work has been supported in part by the Croatian Science Foundation under the project No. 2753.

References

[1] G.A. Harris, A.S. Galhena, F.M. Fernandez, Ambient sampling/ionization mass spectrometry: applications and current trends, Anal. Chem. 83 (2011) 4508–4538.
[2] R.M. Alberici, R.C. Simas, G.B. Sanvido, W. Romão, P.M. Lalli, M. Benassi, I.B.S. Cunha, M.N. Eberlin, Ambient mass spectrometry: bringing MS into the "real world", Anal. Bioanal. Chem. 398 (2010) 265–294.
[3] Z. Takats, J.M. Wiseman, R.G. Cooks, Ambient mass spectrometry using desorption electrospray ionization (DESI): instrumentation, mechanisms and applications in forensics, chemistry, and biology, J. Mass Spectrom. 40 (2005) 1261–1275.
[4] R.G. Cooks, Z. Ouyang, Z. Takáts, J.M. Wiseman, Ambient mass spectrometry, Science 311 (2006) 1566–1570.
[5] A. Venter, M. Neflieu, R.G. Cooks, Ambient desorption mass spectrometry, Trends Anal. Chem. 27 (2008) 284–290.

[6] G.J. Van Berkel, S.P. Pasilis, O. Ovchinnikova, Established and emerging atmospheric pressure surface sampling/ionization techniques for mass spectrometry, J. Mass Spectrom. 43 (2008) 1161–1180.
[7] G.A. Harris, L. Nyadong, F.M. Fernandez, Recent developmentsin ambient ionization techniques for analytical mass spectrometry, Analyst 133 (2008) 1297–1301.
[8] N.E. Manincke, J.M. Wiseman, D.R. Ifa, R.G. Cooks, Desorption electrospray ionization (DESI) mass spectrometry and tandem mass spectrometry (MS/MS) of phospholipids and sphingolipids: ionization, adduct formation, and fragmentation, J. Am. Soc. Mass Spectrom. 19 (2008) 531–543.
[9] H. Chen, G. Gamez, R. Zenobi, What can we learn from ambient ionization techniques? J. Am. Soc. Mass Spectrom. 20 (2009) 1947–1963.
[10] D.R. Ifa, A.U. Jackson, G. Paglia, R.G. Cooks, Forensic applications of ambient ionization mass spectrometry, Anal. Bioanal. Chem. 394 (2009) 1995–2008.
[11] D.J. Weston, Ambient ionization mass spectrometry: current understanding of mechanistic theory; analytical performance and applications areas, Analyst 135 (2010) 661–668.
[12] D.R. Ifa, C. Wu, Z. Ouyang, R.G. Cooks, Desorption electrospray ionization and other ambient ionization methods: current progress and preview, Analyst 135 (2010) 669–681.
[13] H. Chen, N.N. Talaty, Z. Takats, R.G. Cooks, Desorption electrospray ionization mass spectrometry for high-throughput analysis of pharmaceutical samples in the ambient environment, Anal. Chem. 77 (2005) 6915–6927.
[14] P. Nemes, A. Vertes, Ambient mass spectrometry for in vivo local analysis and in situ molecular tissue imaging, Trends Anal. Chem. 34 (2012) 22–34.
[15] Y.S. Shin, B. Drolet, R. Mayer, K. Dolence, F. Basile, Desorption electrospray ionization-mass spectrometry of proteins, Anal. Chem. 79 (2007) 3514–3518.
[16] T. Kauppila, J.M. Wiseman, R.A. Ketola, T. Kotiaho, R.G. Cooks, R. Kostiainen, Desorption electrospray ionization mass spectrometry for the analysis of pharmaceuticals and metabolites, Rapid Commun. Mass Spectrom. 20 (2006) 387–392.
[17] A.U. Jackson, S.R. Werner, N. Talaty, Y. Song, K. Campbell, R.G. Cooks, J.A. Morgan, Targeted metabolomic analysis of *Escherichia coli* by desorption electrospray ionization and extractive electrospray ionization mass spectrometry, Anal. Biochem. 375 (2008) 272–281.
[18] I. Cotte-Rodriguez, H. Hernandez-Soto, H. Chen, R.G. Cooks, In situ trace detection of peroxide explosives by desorption electrospray ionization and desorption atmospheric pressure chemical ionization, Anal. Chem. 80 (2008) 1512–1519.
[19] N. Na, C. Zhang, M. Zhao, S. Zhang, C. Yang, X. Fang, X. Zhang, Direct detection of explosives on solid surfaces by mass spectrometry with an ambient ion source based on dielectric barrier discharge, J. Mass Spectrom. 42 (2007) 1079–1085.
[20] Z. Takats, J.M. Wiseman, B. Gologan, R.G. Cooks, Mass spectrometry sampling under ambient conditions with desorption electrospray ionization, Science 306 (2004) 471–473.
[21] R.B. Cody, J.A. Laramee, H.D. Durst, Versatile new ion source for the analysis of materials in open air under ambient conditions, Anal. Chem. 77 (2005) 2297–2302.
[22] N. Na, M.X. Zhao, S.C. Zhang, C.D. Yang, X.R. Zhang, Development of a dielectric barrier discharge ion source for ambient mass spectrometry, J. Am. Soc. Mass Spectrom. 18 (2007) 1859–1862.
[23] J.D. Harper, N.A. Charipar, C.C. Mulligan, X.R. Zhang, R.G. Cooks, Z. Ouyang, Low-temperature plasma probe for ambient desorption ionization, Anal. Chem. 80 (2008) 9097–9104.
[24] S. Soparawalla, F.K. Tadjimukhamedov, J.S. Wiley, Z. Ouyang, R.G. Cooks, *In situ* analysis of agrochemical residues on fruit using ambient ionization on a handheld mass spectrometer, Analyst 136 (2011) 4392–4396.
[25] L.V. Ratcliffe, F.J.M. Rutten, D.A. Barrett, T. Whitmore, D. Seymour, C. Greenwood, Y. Aranda-Gonzalvo, S. Robinson, M. McCoustra, Surface analysis under ambient conditions using plasma-assisted desorption/ionization mass spectrometry, Anal. Chem. 79 (2007) 6094–6101.
[26] T.M. Brewer, J.R. Verkouteren, Atmospheric identification of active ingredients in over-the-counter pharmaceuticals and drugs of abuse by atmospheric pressureglow discharge mass spectrometry (APGD-MS), Rapid Commun. Mass Spectrom. 25 (2011) 2407–2417.
[27] J. Kratzer, Z. Mester, R.E. Sturgeon, Comparison of dielectric barrier discharge, atmospheric pressure radiofrequency-driven glow discharge and direct analysis in realtime sources for ambient mass spectrometry of acetaminophen, Spectrochim. Acta B 66 (2011) 594–603.
[28] G.C.Y. Chan, J.T. Shelley, A.U. Jackson, J.S. Wiley, C. Engelhard, R.G. Cooks, G.M. Hieftje, Spectroscopic plasma diagnostics on a low-temperature plasma probe for ambient mass spectrometry, J. Anal. At. Spectrom. 26 (2011) 1434–1444.
[29] G.C.Y. Chan, J.T. Shelley, J.S. Wiley, C. Engelhard, A.U. Jackson, R.G. Cooks, G.M. Hieftje, Elucidation of reaction mechanisms responsible for afterglow and reagent-ion formation in the low-temperature plasma probe ambient ionization source, Anal. Chem. 83 (2011) 3675–3686.
[30] M.S. Heywood, N. Taylor, P.B. Farnsworth, Measurement of helium metastable atom densities in a plasma-based ambient ionization source, Anal. Chem. 83 (2011) 6493–6499.
[31] S.B. Olenici-Craciunescu, S. Müller, A. Michels, V. Horvatic, C. Vadla, J. Franzke, Spatially resolved spectroscopic measurements of a dielectric barrier discharge plasma jet applicable for soft ionization, Spectrochim. Acta B 66 (2011) 268–273.
[32] J.T. Shelley, G.C.-Y. Chan, G.M. Hieftje, Understanding the flowing atmospheric-pressure afterglow (FAPA) ambient ionization source through optical means, J. Am. Soc. Mass Spectrom. 23 (2012) 407–417.
[33] S. Müller, T. Krähling, D. Veza, V. Horvatic, C. Vadla, J. Franzke, Operation modes of the helium dielectric barrier discharge for soft ionization, Spectrochim. Acta B 85 (2013) 104–111.
[34] V. Horvatic, S. Müller, D. Veza, C. Vadla, J. Franzke, Atmospheric helium capillary dielectric barrier discharge for soft ionization: determination of atom number densities in the lowest excited and metastable states, Anal. Chem. 86 (2014) 857–864.
[35] V. Horvatic, S. Müller, D. Veza, C. Vadla, J. Franzke, Atmospheric helium capillary dielectric barrier discharge for soft ionization: broadening of spectral lines, gas temperature and electron number density, J. Anal. At. Spectrom. 29 (2014) 498–505.
[36] T. Martens, A. Bogaerts, W.J.M. Brok, J.V. Dijk, The dominant role of impurities in the composition of high pressure noble gas plasmas, Appl. Phys. Lett. 92 (2008) 041504(1)-041504(4).
[37] J.H. Gross, Polydimethylsiloxane-based wide-range mass calibration for direct analysis in real-time mass spectrometry, Anal. Bioanal. Chem. 405 (2013) 8663–8668.
[38] E.S. Chernetsova, G.E. Morlock, I.A. Revelsky, DART mass spectrometry and its applications in chemical analysis, Russ. Chem. Rev. 80 (2011) 235–255.
[39] J.H. Gross, Direct analysis in real time—a critical review on DART-MS, Anal. Bioanal. Chem. 406 (2014) 63–80.
[40] F.J. Andrade, J.T. Shelley, W.C. Wetzel, M.R. Webb, G. Gamez, S.J. Ray, G.M. Hieftje, Atmospheric pressure chemical ionization source. 1. Ionization of compounds in the gas phase, Anal. Chem. 80 (2008) 2646–2653.
[41] F.J. Andrade, J.T. Shelley, W.C. Wetzel, M.R. Webb, G. Gamez, S.J. Ray, G.M. Hieftje, Atmospheric pressure chemical ionization source. 2. Desorption-ionization for the direct analysis of solid compounds, Anal. Chem. 80 (2008) 2654–2663.
[42] M.C. Jecklin, G. Gamez, D. Touboul, R. Zenobi, Atmospheric pressure glow discharge desorption mass spectrometry for rapid screening of pesticides in food, Rapid Commun. Mass Spectrom. 22 (2008) 2791–2798.
[43] J. Shelley, J. Wiley, G.Y. Chan, G. Schilling, S. Ray, G. Hieftje, Characterization of direct-current atmospheric-pressure discharges useful for ambient desorption/ionization mass spectrometry, J. Am. Soc. Mass Spectrom. 20 (2009) 837–844.
[44] M.C. Jecklin, G. Gamez, R. Zenobi, Fast polymer fingerprinting using flowing afterglow atmospheric pressure glow discharge mass spectrometry, Analyst 134 (2009) 1629–1636.
[45] N. Zhang, Y. Zhou, C. Zhen, Y. Li, C. Xiong, J. Wang, H. Li, Z. Nie, Structural characterization of synthetic polymers using thermal-assisted atmospheric pressure glow discharge mass spectrometry, Analyst 137 (2012) 5051–5056.
[46] C.N. McEwen, R.G. McKay, B.S. Larsen, Analysis of solids, liquids, and biological tissues using solids probe introduction at atmospheric pressure on commercial LC/MS instruments, Anal. Chem. 77 (2005) 7826–7831.
[47] M. Teschke, J. Kedzierski, E.G. Finantu-Dinu, D. Korzec, J. Engemann, High-speed photograph of a dielectric barrier atmospheric pressure plasma jet, IEEE Trans. Plasma Sci. 33 (2005) 310–311.
[48] X. Lu, Z. Jiang, Q. Xiong, Z. Tang, X. Hu, Y. Pan, An 11 cm long atmospheric pressure cold plasma plume for applications of plasma medicine, Appl. Phys. Lett. 92 (2008) (081502(1)-081502(2)).
[49] J.L. Walsh, M.G. Kong, Contrasting characteristics of linear-field and cross-field atmospheric plasma jets, Appl. Phys. Lett. 93 (2008) (111501(1)-111501(3)).
[50] Q. Li, J.T. Li, W.C. Zhu, X.M. Zhu, Y.K. Pu, Effects of gas flow rate on the length of atmospheric pressure nonequilibriumplasma jets, Appl. Phys. Lett. 95 (2009) (141502(1)-141502(3)).
[51] X. Lu, Z. Jiang, Q. Xiong, Z. Tang, Y. Pan, A single electrode room-temperature plasma jet device for biomedical applications, Appl. Phys. Lett. 92 (2008) (151504(1)-151504(3)).
[52] M. Miclea, K. Kunze, G. Musa, J. Franzke, K. Niemax, The dielectric barrier discharge—a powerful microchip plasma for diode laser spectrometry, Spectrochim. Acta B 56 (2001) 37–43.
[53] J.C.T. Eijkel, H. Stoeri, A. Manz, A molecular emission detector on a CIP employing a direct current microplasma, Anal. Chem. 71 (1999) 2600–2606.
[54] J.C.T. Eijkel, H. Stoeri, A. Manz, A dc microplasma on a chip employed as an optical emission detector for gas chromatography, Anal. Chem. 72 (2000) 2547–2552.
[55] U. Engel, A.M. Bilgiç, O. Haase, E. Voges, J.A.C. Broekaert, A microwave-induced plasma based on microstrip technology and its use for the atomic emission spectrometric determination of mercury with the aid of the cold-vapor technique, Anal. Chem. 72 (2000) 193–197.
[56] A. Michels, S. Tombrink, W. Vautz, M. Miclea, J. Franzke, Spectroscopic characterization of a microplasma used as ionization source for ion mobility spectrometry, Spectrochim. Acta B 62 (2007) 1208–1215.
[57] G.A. Eiceman, Z. Karpas, Ion Mobility Spectrometry, 2nd ed. CRC Press, London, UK, 2005.
[58] H.E. Wagner, R. Brandenburg, K.V. Kozlov, A. Sonnenfeld, P. Michel, J.F. Behnke, The barrier discharge: basic properties and applications to surface treatment, Vacuum 71 (2003) 417–436.
[59] M. Endoh, M. Tsuji, Y. Nishimura, Thermal energy charge-transfer reactions: He_2^+ with N_2 and CO, J. Chem. Phys. 79 (1983) 5368–5375.
[60] C. Meyer, S. Müller, B. Gilbert-Lopez, J. Franzke, Impact of homogeneous and filamentary discharge modes on the efficiency of dielectric barrier discharge ionization mass spectrometry, Anal. Bioanal. Chem. 405 (2013) 4729–4735.